Enormous Lithium Isotopic Variations of Abyssal Peridotites Reveal Fast Cooling and Melt/Fluid-Rock Interactions

Ping-Ping Liu[1] [ID], Ju Liang[1], Henry J. B. Dick[2] [ID], Xian-Hua Li[3] [ID], Qiong Chen[4], Hao-Yue Zuo[5], and Jia-Cheng Wu[5] [ID]

[1]Key Laboratory of Orogenic Belts and Crustal Evolution, School of Earth and Space Sciences, Peking University, Beijing, China, [2]Department of Geology and Geophysics, Woods Hole Oceanographic Institution, Woods Hole, MA, USA, [3]Institute of Geology and Geophysics, Chinese Academy of Sciences, Beijing, China, [4]School of Ocean and Earth Science, Tongji University, Shanghai, China, [5]Department of Atmospheric and Oceanic Sciences, School of Physics, Peking University, Beijing, China

Abstract Fast diffusing Li isotopes provide important insights into the "recent" transient events or processes for both modern and ancient times, but questions remain concerning the large Li isotopic variations of mantle peridotites, which greatly hampers their usage as a geochemical tracer. This study investigates in situ Li content and isotopic profiles of the constituent minerals of abyssal peridotites from the Gakkel Ridge and Southwest Indian Ridge. The complicated and large variations of Li isotopic profiles in Clinopyroxene (Cpx) and Orthopyroxene (Opx) indicate Li isotopic disequilibrium at millimeter scale. The negative correlations of a wide range of Li contents (0.5 to 6.5 ppm) and δ^7Li values (−10 to +20‰) of olivine, Opx and Cpx grains/relicts, trace element zoning of Cpx, the occurrence of plagioclase, olivine serpentinization along cracks, together with numerical modeling demonstrate the observed Li characteristics to be a manifestation of high-temperature mineral-melt Li diffusion during melt impregnation overprinted by low-temperature mineral-fluid Li diffusion during dissolution and serpentinization. The preservation of the Li isotopic diffusion profiles requires rapid cooling of 0.3–5°C/year after final-stage melt impregnation at the Moho boundary, which is consistent with the low temperature at very slow spreadin g ridges caused by conductive cooling. Compared with the well-studied melt-rock interaction process, our study indicates that low-temperature fluid-rock interaction can induce Li diffusion even in the visibly unaltered mineral relics of partially altered rocks.

1. Introduction

The Li isotopic composition of the Earth's mantle reservoir is important for understanding planetary differentiation, crust-mantle interaction, and partial melting (e.g., Jeffcoate et al., 2007; Rudnick & Ionov, 2007; Su et al., 2014; Tang et al., 2007, 2014). Because of the low mass and large mass difference (~16%) between ^6Li and ^7Li, both these isotopes have high diffusivity and highly variable isotopic compositions in mantle peridotites compared with heavier stable isotopes such as Fe and Mg (e.g., Teng et al., 2017; Tomascak, 2004). The large Li isotopic variations in the constituent minerals are commonly in disequilibrium and negatively correlated with Li contents (e.g., Tomascak et al., 2016). The mechanism of Li isotopic fractionation in mantle peridotites is still not fully understood and may include (1) diffusion-controlled silicate melt-rock and carbonatite melt-rock metasomatism (Rudnick & Ionov, 2007; Su et al., 2014; Woodland et al., 2004), (2) cooling-induced interdiffusion between coexisting minerals (Coogan et al., 2005; Gao et al., 2011; Ionov & Seitz, 2008), and (3) metasomatism by dehydration fluids from subducted oceanic slabs (e.g., Gu et al., 2016).

Abyssal peridotites commonly exposed in slow-spreading mid-ocean ridges are unlikely to be affected by subduction zone processes and can therefore pinpoint specific mechanisms leading to Li isotopic variations. Here, we present a systematic in situ Li elemental and isotopic study of six slightly altered abyssal peridotites from the ultra-slow spreading Gakkel Ridge and Southwest Indian Ridge (SWIR). Our study demonstrates a negative correlation between Li content and δ^7Li value in olivine, Cpx and Opx of the studied abyssal peridotites. In Li content versus δ^7Li value diagram, these data form two trends spreading from the pristine mantle value (Li = 1–2 ppm, δ^7Li = 4 ± 2‰; Jeffcoate et al., 2007; Seitz & Woodland, 2000; Seitz et al., 2004).

Combined with petrographic evidence and trace element zoning in Cpx, Li isotopic profiles and numerical modeling are used to propose a two-stage model for the Li variations in the abyssal peridotites.

2. Geological Setting and Samples

The Gakkel Ridge is an ultraslow-spreading ridge in the Arctic Ocean, with a full spreading rate of 8 to 13 mm/year, and extends east for about 1,800 km from the Lena trough, north of Greenland, toward the continental margin of the Laptev Sea (Figure 1a; Thiede et al., 2002). Three distinct magmato-tectonic domains were recognized along the Gakkel Ridge characterized by different abundances of rock types: a western volcanic zone, a central sparsely magmatic zone that is nearly amagmatic, and an eastern zone composed of widely spaced volcanoes (Michael et al., 2003). The SWIR lies between the African and Antarctic plates and spreads at a full rate of 14 to 16 mm/year (DeMets et al., 1990). It extends from the Bouvet triple junction northeastward to the central Indian triple junction (Figure 1b). Peridotites recovered from the ultra-slow spreading Gakkel Ridge and SWIR with thin, or even missing, crust commonly vary from depleted harzburgite to fertile lherzolite and are inferred to have undergone previous melting events prior to the current ridge melting event (Dick et al., 2003; Gao et al., 2016; Michael et al., 2003; Zhou & Dick, 2013).

Six slightly altered abyssal peridotites were investigated for Li isotopes in this study. One sample was collected on cruise Protea Expedition, Leg 5 (Pr) of the RV Melville from the ~140-km long Prince Edward Transform Fault (46.54°S, 33.79°E) (Dick et al., 1984). The other samples were collected at 84.64°N, 4.22°E, 84.83°N, 4.66°E, and 85.44°N, 14.52°E on the Sparsely Magmatic Zone of the Gakkel Ridge during the AMORE Expedition of the USCGC Healy (HLY) and RV Polarstern (PS) (Michael et al., 2003). The abyssal peridotites are mostly composed of olivine, Opx and Cpx (Figures 1c–1h), with minor plagioclase and spinel (Figures 2b and 2d). Most olivine grains contain an ubiquitous microfracture network of black to brown alteration veinlets filled with serpentine, Fe-oxides, and oxidized brown clay (Figures 1 and 2; Liu et al., 2017). Clinopyroxene grains are small, 2–4 mm in size and make up 0 to 22 vol.% of the samples. They are very fresh; some of which contain Opx exsolution lamellae (Figure 2a). Orthopyroxene grains are bigger, 4–5 mm in size and make up 7 to 36 vol.% of the samples. Orthopyroxene grains are mostly fresh (Figure 2b), except those in sample PROT 19-5 that are slightly serpentinized (Figure 2c). Detailed mineralogical, petrographic, and geochemical features of abyssal peridotites in the SWIR and Gakkel Ridge are available in literature (e.g., Dick et al., 2003; Hellebrand et al., 2001; Liu et al., 2008; Michael et al., 2003).

3. Analytical Methods

3.1. Electron Microprobe Analysis

Major element compositions of olivine, Cpx, Opx, spinel, and plagioclase were analyzed using a JEOL JXA-8230 electron probe micro-analyzer (EPMA) in the Department of Earth Sciences, the University of Hong Kong. The analyses were carried out under a voltage of 15 kV and a beam current of 20 nA focused to a spot size of 10 μm. Peak and background counting times for major elements were 10 and 20 s, whereas those for trace elements were 20 and 30 s, respectively. Natural and synthetic oxides were used as standards during the analyses. The precisions of the major and trace element analyses were better than 2% and 5%, respectively. Matrix corrections were performed by the ZAF procedures.

3.2. In Situ LA-ICP-MS Analysis

Trace element compositions of Opx and Cpx were analyzed by a Coherent GeoLasPro 193-nm Laser Ablation system coupled with an Agilent 7700× ICP-MS at the State Key Laboratory of Ore Deposit Geochemistry, Institute of Geochemistry, Chinese Academy of Sciences. USGS standard reference materials of BHVO-2G, BCR-2G, BIR-1G, and NIST610 were used as external standards. Standard ML3B-G was analyzed for quality control. Each analysis includes ~20 s for measuring the gas blank and ~40 s for data acquisition using a spot size of 44 μm at 6 Hz with an energy of ~100 mJ per pulse. In order to correct the time-dependent drift of sensitivity and mass discrimination, two analyses of NIST610 were tested between every 15 analyses. Processing of the LA-ICP-MS data was performed on ICPMSDataCal, an offline data processing software (Liu et al., 2008).
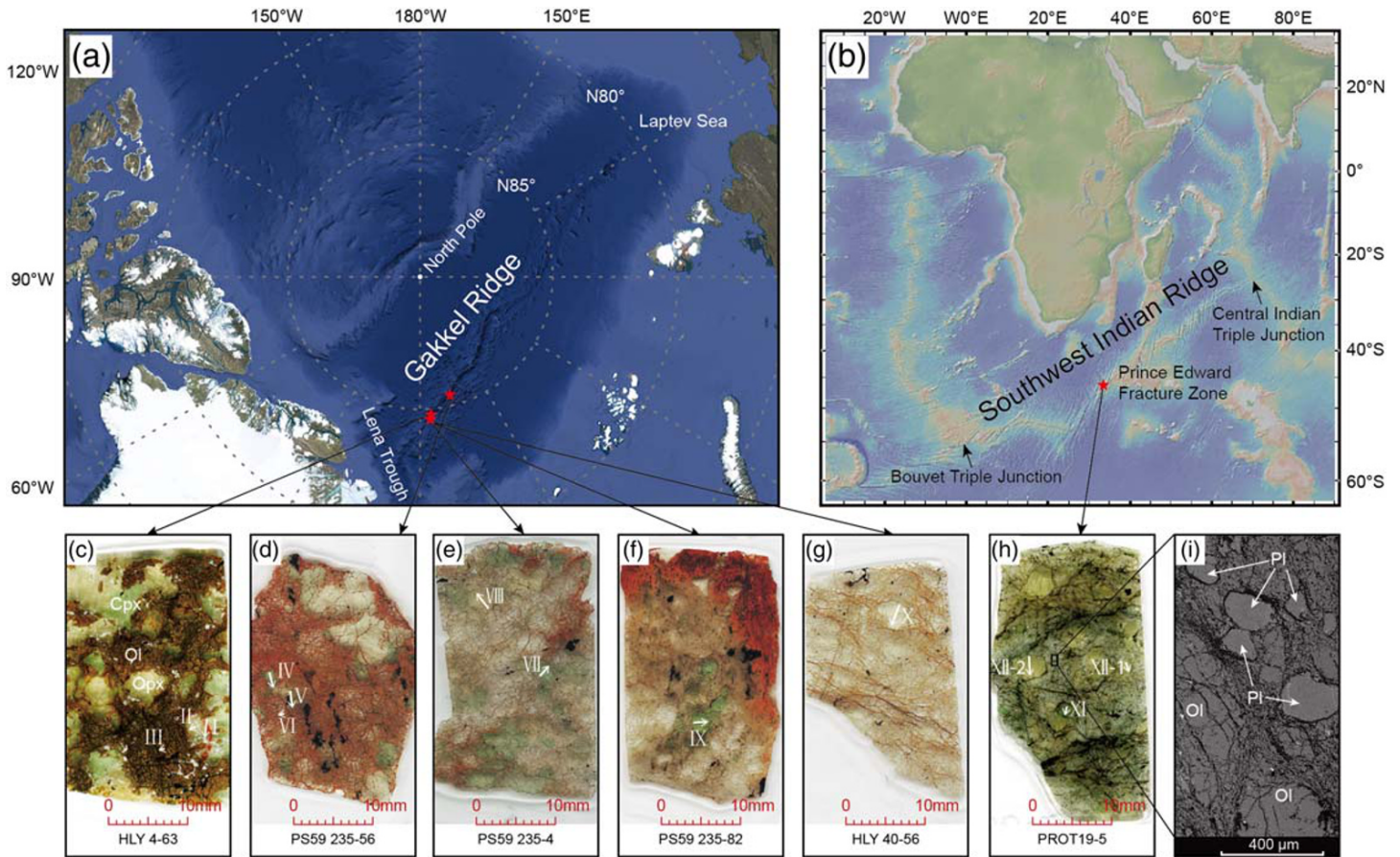
Figure 1. Physiographic and geoid maps of the Gakkel Ridge in Arctic Ocean (a) and the Southwest Indian Ridge (SWIR) in Indian and Atlantic Oceans (b). (c–g) Polished thin sections of abyssal peridotites from the Gakkel Ridge. Coarse mineral grains can be easily identified from the color, where minerals with a light green color are clinopyroxene (Cpx), light yellow color are orthopyroxene (Opx), and the large colorless area with numerous brown to black veinlets are olivine (Ol). (h) Abyssal peridotite from the SWIR. (i) A zoom-in BSE image of Figure 1h showing the microtextures of olivine serpentinization along the cracks and the occurrence of plagioclase (Pl). Roman numbers and arrows in (c)–(h) mark the places where Li isotopic profiles were analyzed.

3.3. In Situ SIMS Analysis

Polished rock slices were vacuum-coated with high-purity gold and analyzed using Cameca IMS-1280HR SIMS at the Institute of Geology and Geophysics, Chinese Academy of Sciences (IGGCAS). The analytical spots were elliptical and ~20 × 30 μm in size. A 60-s presputtering with raster was performed before each analysis. The O^- primary ion beam used was accelerated at 13 kV, with an intensity of about 15 to 30 nA. Positive secondary ions were measured on an ion multiplier in pulse counting mode, with a mass resolution (M/DM) of 1,500 and an energy slit open at 40 eV without any energy offset. The secondary ion beam position in apertures, as well as the magnetic field and the energy offset, were automatically centered before each measurement. Eighty cycles were measured with counting times of 7 and 2 s for ^6Li and ^7Li, respectively, in a single cycle. The measured δ^7Li values are defined as $\delta^7Li = [(^7Li/^6Li)_{sample}/(^7Li/^6Li)_{L-SVEC} - 1] \times 1,000$ relative to units of the standard NIST SRM 8545 (L-SVEC) with $^7Li/^6Li$ ratio of 12.0192. The instrumental mass fractionation is expressed as $\Delta I = \delta^7Li_{SIMS} - \delta^7Li_{MC-ICPMS}$. Standard 06JY31OL with a Mg# of 90.3, lithium concentration of 2.70 ± 0.30 ppm, and δ^7Li of 4.51 ± 0.17‰ was used to calibrate olivine (Su et al., 2015), the instrumental mass fractionation of which is 29.93 ± 0.83‰. Standard 06JY31CPX with a Mg# of 91.1, lithium concentration of 1.16 ± 0.01 ppm, and δ^7Li of −2.37 ± 0.23‰ was used to calibrate Cpx (Su et al., 2015), the instrumental mass fractionation of which is 41.36 ± 0.95‰. Standard 06JY31OPX with a Mg# of 90.8, lithium concentration of 1.33 ± 0.12 ppm, and δ^7Li of −0.19 ± 0.11‰ was used to calibrate Opx (Su et al., 2015), the instrumental mass fractionation of which is 37.06 ± 1.11‰. Lithium concentrations were calculated on the basis of $^7Li^+$ count rates (cps/nA) relative to the standard.
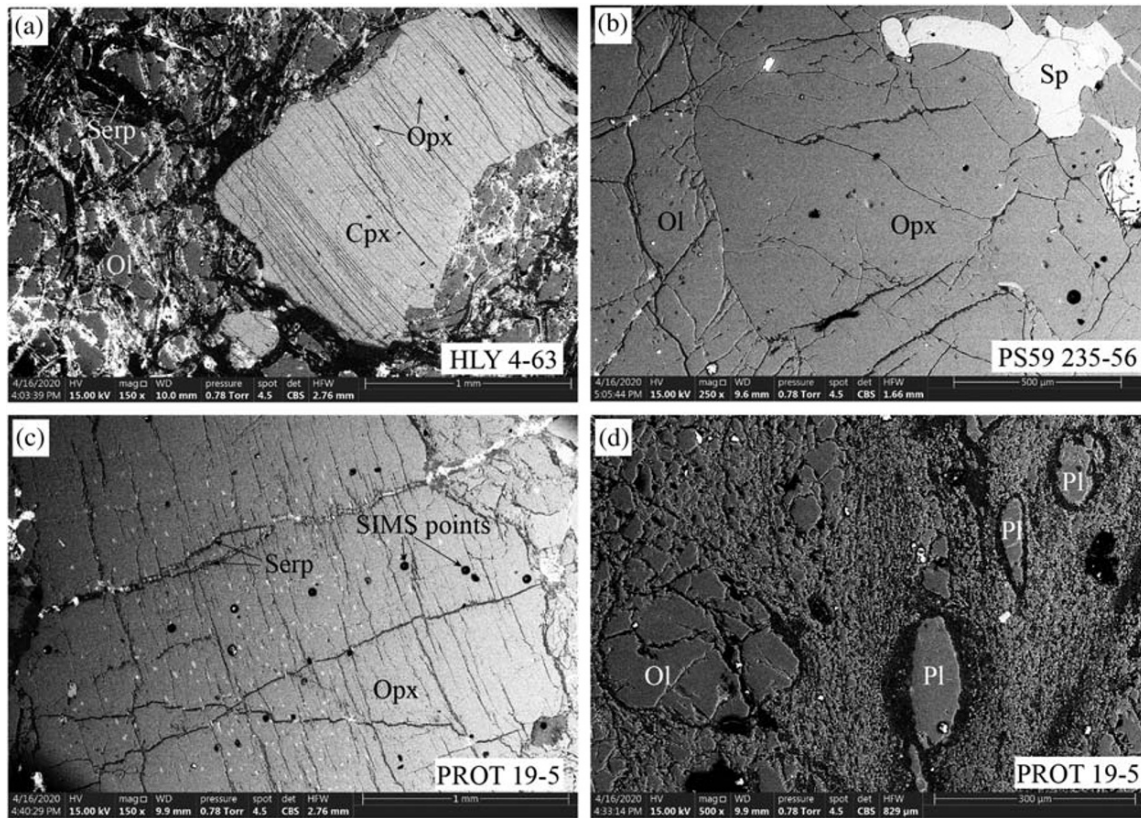
Figure 2. Back-scattered electron images showing mineral textures of the abyssal peridotites. Sp-spinel. Other mineral abbreviations can be referred to Figure 1.

The detection limit of Li is <1 ppb. Matrix effects caused by the discrepancy of Fo content of the olivine standard and the samples were carefully calibrated (Su et al., 2015). To be conservative, the uncertainties we reported are 2σ errors of single spot analyses (Table 1). Detailed analytical procedures can be referred to Decitre et al. (2002) and Li et al. (2011).

4. Results

4.1. Mineral Major and Trace Element Composition

Olivine, Opx, and Cpx in the peridotites have a relatively narrow range of Mg# (Mg/(Mg + Fe) × 100) from 89.5 to 92.0, 89.9 to 92.2, and 89.5 to 92.7, respectively, typical of abyssal peridotites worldwide. Cr#s (Cr/(Cr + Al) × 100) of spinel vary from 13 to 54. Plagioclase in sample PROT 19-5 has variable anorthite contents ranging from 73.5 to 84 (Table S1). These rocks have undergone ~3% to 17% partial melting assuming a primitive upper mantle composition (Figure 3a; Hellebrand et al., 2001).

Clinopyroxene and Opx from three representative peridotite samples with smallest and largest Li isotopic variations were chosen for in situ trace element analyses. Cpx and Opx in these samples exhibit different extents of LREE depletion in contrast to their flat HREE (Figures 4a–4c). Clinopyroxene from samples PS59 235-4 and PS59 235-56 have REE contents similar to or slightly higher than those of the least depleted Gakkel Ridge peridotites (Figures 4a and 4b), whereas Cpx from sample PROT 19-5 has slight LREE enrichment compared with those in abyssal peridotites from the SWIR (Figure 4c). Compositional variations of Cpx between samples are relatively large, with the concentration of La, for example, varying by 10 times (Figures 4a–4c). Compositional zoning was observed in almost all Cpx grains analyzed, characterized by increased Y and Zr contents toward the rim (Figures 4d–4f). In the plots of Ti versus Zr content of Cpx, the peridotites have undergone ~5% to 12% fractional melting of a primitive upper mantle, consistent with those inferred from Cr#s of spinel (Figures 3a and 3b).

Table 1
In Situ Li Concentration and $\delta^7 Li$ Value of the Studied Peridotites

Sample	Mineral/ Whole rock[a]	Profile no.	$\delta^7 Li$ (‰)	2σ	Li (ppm)	2σ
HLY 4–63	Cpx grain 1@1rim	I	−3.77	1.20	2.68	0.04
	Cpx grain 1@2mantle		−5.17	1.08	2.41	0.04
	Cpx grain 1@3core		−4.18	1.06	2.13	0.04
	Cpx grain 1@4core		−4.84	1.04	2.24	0.04
	Cpx grain 1@5mantle		−4.60	1.12	2.89	0.06
	Cpx grain 1@6rim		−2.97	1.06	2.16	0.04
	Opx grain 1		−3.54	1.60	0.81	0.02
	Opx grain 2		−3.81	1.28	1.30	0.02
	Opx grain 3@1rim	II	−2.67	1.44	0.96	0.02
	Opx grain 3@2mantle		−0.41	1.38	1.08	0.02
	Opx grain 3@3core		1.02	1.36	1.10	0.02
	Opx grain 3@4mantle		0.64	1.34	1.13	0.02
	Opx grain 3@5rim		−3.79	1.36	1.09	0.02
	Ol grain 1		5.78	1.12	1.74	0.04
	Ol grain 2		3.18	1.10	1.84	0.04
	Ol grain 3@1rim	III	2.86	0.98	2.27	0.04
	Ol grain 3@2core		4.47	1.12	1.80	0.04
	Ol grain 3@3core		4.87	1.12	1.85	0.04
	Ol grain 3@4rim		3.45	1.08	1.89	0.02
	Whole rock		2.13		1.82	
PS59 235–56	Cpx grain 1@1		−6.69	0.70	5.06	0.08
	Cpx grain 2@1		−6.86	0.68	5.46	0.08
	Cpx grain 3@1rim	IV	−4.58	0.64	6.15	0.10
	Cpx grain 3@2mantle		−3.89	0.68	5.46	0.08
	Cpx grain 3@3core		−4.78	0.66	5.61	0.10
	Cpx grain 3@4core		−4.25	1.76	6.67	0.26
	Cpx grain 3@5mantle		−6.31	0.64	6.16	0.10
	Cpx grain 3@6rim		−5.47	0.82	4.31	0.08
	Opx grain 1		−3.06	1.16	1.60	0.02
	Opx grain 2		−3.42	1.26	1.39	0.02
	Opx grain 3@1rim	V	−2.27	1.06	2.01	0.04
	Opx grain 3@2mantle		−2.34	1.06	2.24	0.04
	Opx grain 3@3core		−3.35	1.08	1.81	0.04
	Opx grain 3@4mantle		−3.44	1.04	2.30	0.04
	Opx grain 3@5rim		−4.31	1.00	2.12	0.04
	Ol grain 1		15.20	1.60	0.94	0.02
	Ol grain 2		14.50	1.54	0.99	0.02
	Ol grain 3@1rim	VI	13.43	1.52	1.12	0.02
	Ol grain 3@2mantle		10.26	1.52	1.20	0.02
	Ol grain 3@3core		12.44	1.40	1.17	0.02
	Ol grain 3@4mantle	VI	11.13	1.46	1.17	0.02
	Ol grain 3@5rim		9.79	1.54	1.21	0.02
	Whole rock		5.20		1.48	
PS59 235–4	Cpx grain 1		−10.25	0.78	3.91	0.06
	Cpx grain 2@1rim	VII	−7.20	1.00	2.54	0.04
	Cpx grain 2@2core		−9.46	0.80	3.79	0.06
	Cpx grain 2@3core		−8.04	0.76	3.97	0.06
	Cpx grain 2@4rim		−10.60	0.72	4.44	0.06
	Opx grain 1		−0.78	1.22	1.20	0.02
	Opx grain 2		−0.42	1.20	1.26	0.02
	Opx grain 3@1rim	VIII	0.88	1.30	1.07	0.02
	Opx grain 3@2core		−1.30	1.46	0.83	0.02
	Opx grain 3@3core		−1.69	1.32	1.01	0.02
	Opx grain 3@4rim		−0.73	1.20	1.24	0.02
	Ol grain 1		14.33	1.42	1.06	0.02
	Ol grain 2		12.76	1.30	1.23	0.02
	Ol grain 3		14.28	1.32	1.19	0.02
	Ol grain 4		13.50	1.34	1.15	0.02
	Ol grain 5		18.74	1.34	1.16	0.02

Table 1
Continued

Sample	Mineral/ Whole rock[a]	Profile no.	δ^7Li (‰)	2σ	Li (ppm)	2σ
	Ol grain 6		12.07	1.40	1.06	0.02
	Whole rock		1.07		1.72	
PS59 235–82	Cpx grain 1		2.20	0.74	3.81	0.06
	Cpx grain 2@1rim	IX	−5.59	0.70	4.71	0.08
	Cpx grain 2@2core		−8.66	0.80	3.65	0.06
	Cpx grain 2@3core		−7.42	0.62	6.03	0.10
	Cpx grain 2@4rim		−6.09	0.76	4.10	0.08
	Opx grain 1		0.19	0.80	2.80	0.04
	Opx grain 2		−0.02	0.90	2.22	0.04
	Ol grain 1		3.20	1.22	1.68	0.02
	Ol grain 2		3.37	1.10	1.73	0.02
	Whole rock		0.59		2.62	
HLY 40–56	Opx grain 1		−3.07	1.06	1.79	0.02
	Opx grain 2@1rim	X	−1.09	1.18	1.09	0.02
	Opx grain 2@2core		−2.30	1.08	1.32	0.02
	Opx grain 2@3core		−1.47	1.36	1.20	0.02
	Opx grain 2@4rim		−2.37	1.30	1.29	0.02
	Ol grain 1		2.52	1.24	1.79	0.02
	Ol grain 2		4.53	1.34	1.30	0.02
	Ol grain 3		5.30	1.20	1.55	0.02
	Ol grain 4		4.12	1.18	1.54	0.02
	Whole rock		3.55		1.52	
PROT 19–5	Cpx grain 1@1rim	XI	−1.56	0.90	3.05	0.04
	Cpx grain 1@2core		−2.02	0.80	3.73	0.06
	Cpx grain 1@3core		−3.43	1.10	3.09	0.04
	Cpx grain 1@4rim		−0.24	0.96	3.90	0.06
	Opx grain 1		0.48	2.46	0.98	0.02
	Opx grain 3@1rim	XII-1	10.12	1.22	1.49	0.02
	Opx grain 3@2mantle		3.56	1.40	0.94	0.02
	Opx grain 3@3core		4.65	1.46	0.86	0.02
	Opx grain 3@4mantle		9.84	1.54	0.79	0.02
	Opx grain 3@5rim		18.46	1.60	0.73	0.02
	Opx grain 2@1rim	XII-2	17.37	2.36	0.44	0.02
	Opx grain 2@2mantle		9.92	1.78	1.18	0.02
	Opx grain 2@3core		11.98	2.36	1.51	0.08
	Opx grain 2@4mantle		14.76	1.24	1.17	0.02
	Opx grain 2@5rim		8.45	1.22	1.20	0.02
	Ol grain 1		4.76	1.14	2.25	0.04
	Ol grain 2		4.96	0.88	2.68	0.04
	Ol grain 3		3.21	0.92	2.62	0.04
	Ol grain 4		1.75	0.90	2.52	0.04
	Ol grain 5		7.77	1.12	2.03	0.02
	Whole rock		4.53		2.29	

Note. Cpx grain 1@1 to @4 represent a transect profile of a Cpx grain, the same to Opx and Ol. Rim, mantle and core represent the relative positions along the cross section. Ol = olivine, Opx = orthopyroxene, Cpx = clinopyroxene.
[a]Li content and δ^7Li value of the whole rock are calculated according to the mineral compositions and modal proportions.

4.2. Lithium Contents and Isotopes

Olivine, Opx, and Cpx in the peridotites have Li concentrations varying from 0.94 to 3.82 ppm, 0.44 to 2.80 ppm, and 2.13 to 6.67 ppm, respectively (Table 1). Orthopyroxene and Cpx show concave and convex zoning patterns, some symmetric, and some asymmetric (Figure 5). The two Li isotopic profiles of small olivine relicts bounded by cracks are also heterogeneous (Figure 5, III and VI). In most samples, olivine has Li concentrations similar to or slightly lower than Opx but significantly (1–5 ppm) lower than Cpx (Figure 6a). Most of the olivine grains have Li contents within or slightly beyond the range of pristine olivine (Li = 1–2 ppm) of the equilibrated mantle peridotites, whereas Li content of Cpx is consistently higher than
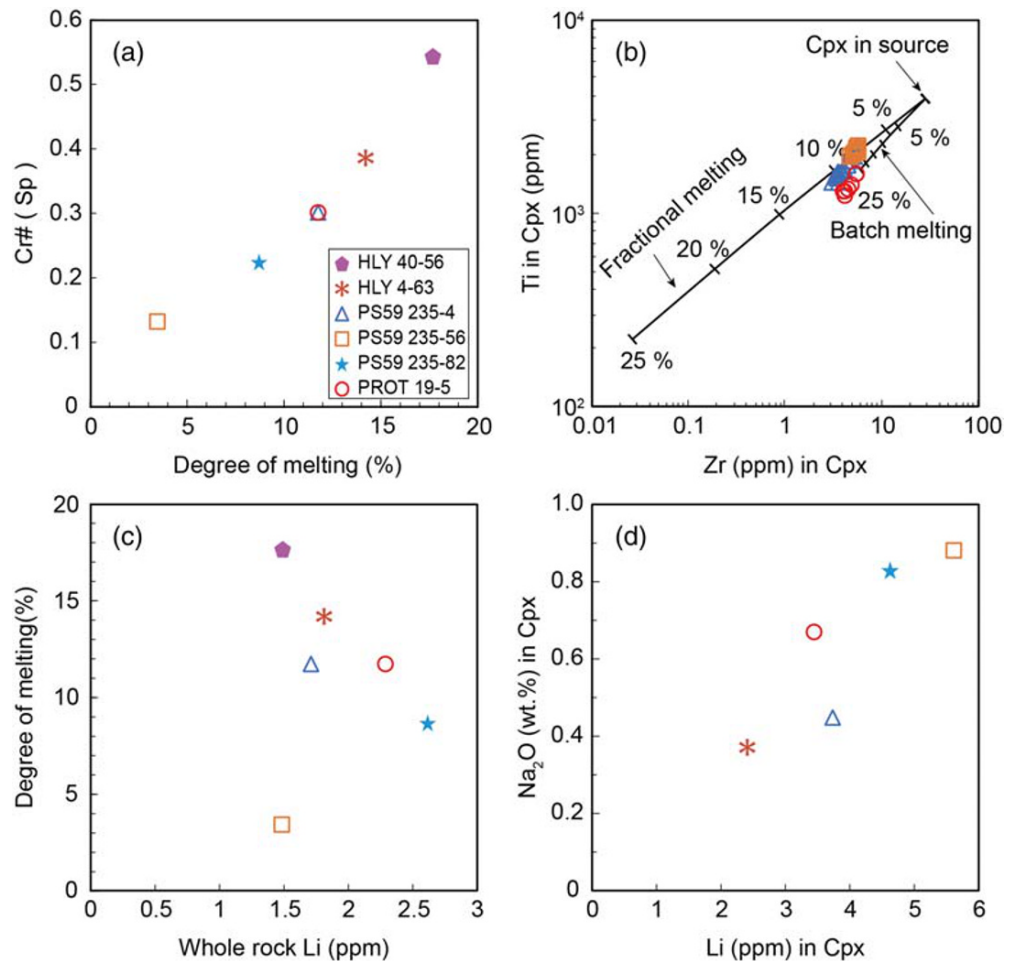
Figure 3. Plots of (a) Cr# of spinel versus degree of melting calculated according to Hellebrand et al. (2001). (b) Ti versus Zr content in Cpx, (c) degree of melting versus calculated whole-rock Li content and (d) Na$_2$O versus Li content in Cpx.

that from the pristine mantle peridotites (Figure 6a; Jeffcoate et al., 2007; Seitz & Woodland, 2000). Whole-rock Li contents calculated by the Li contents in the constituting minerals and their relative proportions show no correlation with Cr#s of spinel (Figure 3c). Lithium content of Cpx has a positive correlation with its Na$_2$O content (Figure 3d). The Li contents of olivine, Opx, and Cpx in this study partially overlap and overall spread a larger range than those reported elsewhere from the SWIR and Gakkel Ridge (Decitre et al., 2002; Gao et al., 2011).

Olivine, Opx, and Cpx have δ^7Li values ranging from 1.75‰ to 18.74‰, −4.31‰ to 18.46‰, and −10.60‰ to −0.24‰, respectively (Table 1). Lithium isotopic profiles of Opx and olivine display both concave and convex zoning patterns, either in the same or opposite trends with that of Li contents. Li isotopic profiles of Cpx, however, are mostly concave in shape (Figure 5). In most samples, the δ^7Li values follow the order of δ^7Li$_{Olivine}$ > δ^7Li$_{Opx}$ > δ^7Li$_{Cpx}$, except sample PROT 19-5, which has δ^7Li$_{Opx}$ > δ^7Li$_{Olivine}$ > δ^7Li$_{Cpx}$ (Figure 6a). Intermineral Li isotopic variations in single hand sample are mostly small (<5‰), except Opx in sample PROT 19-5, which has δ^7Li varying from ~0‰ to 19‰. The range of Li content and isotopes of different minerals in this study overlap with previously reported ones by Gao et al. (2011) but very different from that in Decitre et al. (2002), which have Li content less than 1 ppm and δ^7Li values mostly higher than that of the pristine mantle (Figure 6b). Overall, the δ^7Li values are negatively correlated with the Li contents in our data and for peridotites previously reported from different sections of the same ridges (Decitre et al., 2002; Gao et al., 2011).
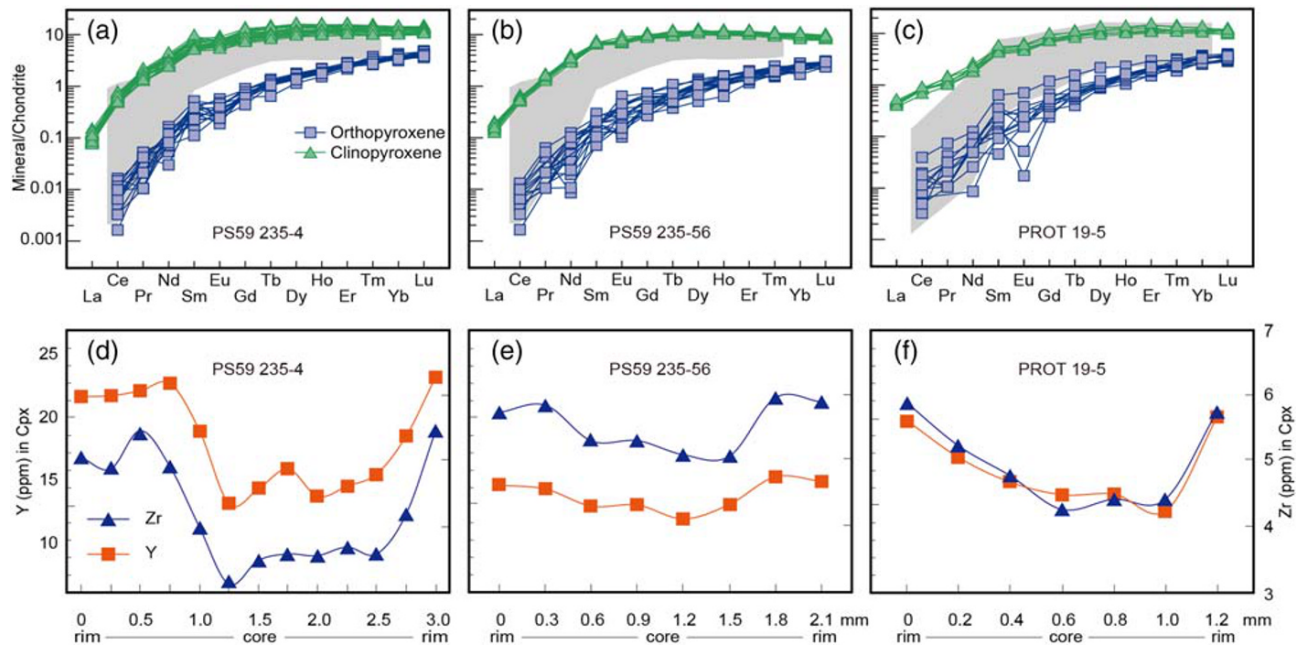
Figure 4. (a–c) Chondrite-normalized rare earth element diagrams of Opx and Cpx (Sun & McDonough, 1989). (d–f) Y and Zr concentration zoning of Cpx. The gray fields in (a) and (b) represent previously reported compositions of Gakkel ridge Cpx (Hellebrand et al., 2005; D'Errico et al., 2016), whereas that in (c) represents Cpx from Atlantis II fracture zone peridotites of SWIR (Johnson & Dick, 1992).

5. Discussion

Compared with the pristine mantle peridotites, the large variations of Li isotopes and Li contents in olivine, Opx, and Cpx of the abyssal peridotites indicate disequilibrium Li isotopic fractionation (Figure 6a). The negative correlations between Li contents and Li isotopes in the silicates are consistent with diffusion-driven kinetic fractionation in that the diffusivity is inversely correlated with the mass of an isotope (Parkinson et al., 2007; Richter et al., 2003; Tang et al., 2007). However, the majority of olivine has lower Li contents and higher δ^7Li values than the pristine mantle olivine (~2 ppm, 4 ± 1‰), whereas the Cpx has higher Li content and lower δ^7Li values than the pristine mantle Cpx (~1 ppm, 4 ± 1‰). The characteristics of Li contents and isotopes reflect the processes involved in the petrogenesis of the abyssal peridotites.

Before the exhumation of mantle peridotites by detachment faulting on the rift valley wall, they underwent partial melting and melt-rock reaction in the asthenosphere and lithosphere, followed by melt impregnation through diffusive porous flow or channelized melt flow when being uplifted to the thermal boundary layer below Moho (e.g., Aharonov et al., 1995; Dick, 1989; Niu, 1997; Niu et al., 1997; Seyler & Brunelli, 2018; Warren & Shimizu, 2010). With continued upwelling, circulation of hydrothermal fluids along the fault systems in very slow-spreading ridges can reach the Moho boundary so that enhanced conductive cooling and high-temperature alteration can occur at the Moho boundary (Cannat et al., 2003; Tao et al., 2020). Since partial melting does not fractionate Li isotopes (Figure 3c; Tomascak et al., 1999; Seitz et al., 2004), and Li can re-equilibrate in several days to years at mantle temperatures because of its fast diffusivity (Dohmen et al., 2010; Parkinson et al., 2007), peridotites in the melting region are considered to be in Li isotopic equilibrium. The isotopically "unequilibrated" peridotites were considered as being formed through modification of pristine mantle peridotites by secondary low-temperature or transient high-temperature processes such as melt metasomatism, reaction or cooling that could have happened shortly before they cooled down and uplifted onto the seafloor (e.g., Parkinson et al., 2007; Rudnick & Ionov, 2007; Seitz & Woodland, 2000).

5.1. Cooling-Induced Li Isotopic Fractionation

Cooling of magmatic rocks has been proved to be an important process for Li diffusion between coexisting minerals and between minerals and matrix (e.g., Beck et al., 2006; Coogan et al., 2005; Gallagher & Elliott, 2009). For example, subsolidus Li diffusion from groundmass was recorded in Li contents and
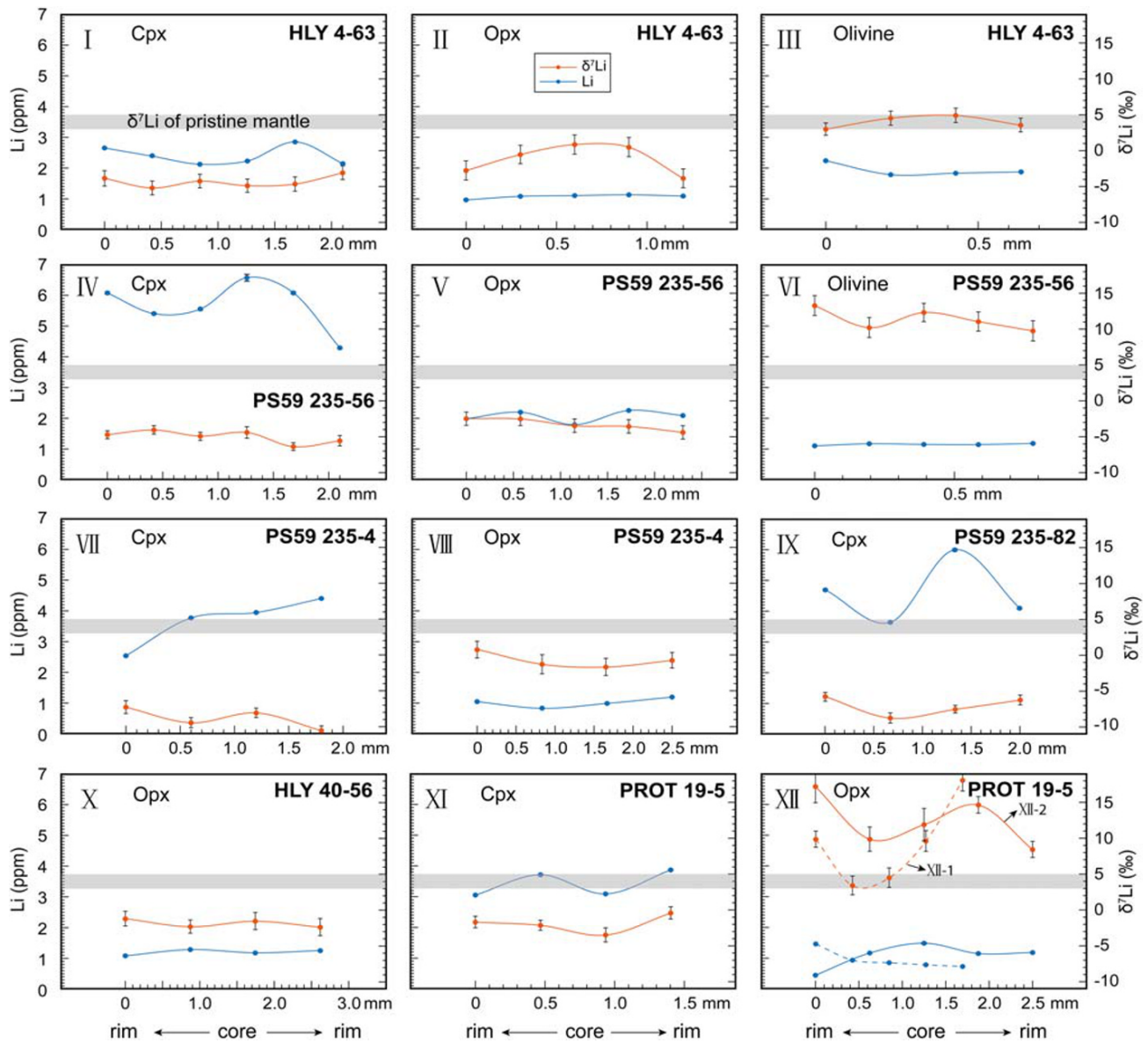
Figure 5. Li content and isotopic profiles of Cpx, Opx, and olivine. The roman numbers in each panel correspond to the numbers and profiles shown in Figure 1c–1h and in Table 1. The errors shown on Li isotopic profiles are 2σ errors.

isotopic zoning of phenocrysts in volcanic rocks (Beck et al., 2006; Gallagher & Elliott, 2009). Moreover, the partitioning of Li between plagioclase and Cpx is experimentally proven to be sufficiently dependent on temperature that Li diffusion from plagioclase to Cpx during cooling can be used to calculate the cooling rate of a rock (Coogan et al., 2005). Based on this and the negative correlation between Li content and isotopes in Cpx and olivine, Gao et al. (2011) proposed that Li diffusion between olivine and Cpx can be comparable to that of plagioclase and Cpx and that the contrasting Li behavior in olivine and Cpx in Gakkel Ridge peridotites was due to cooling-induced Li diffusion from olivine to Cpx. In their numerical modeling, hypothetical change of $Kd^{Li}_{olivine\text{-}cpx}$ from 1.82 at 1200°C to 0.04 at 700°C would result in a maximum $\Delta^7Li_{Olivine\text{-}Cpx}$ value of ~9‰, whereas a lower temperature dependence of $Kd^{Li}_{ol\text{-}cpx}$ (1.82 to 0.89 from 1200°C to 700°C) can only produce a maximum $\Delta^7Li_{Ol\text{-}Cpx}$ variation of ~2‰ (Gao et al., 2011). These modeling Li isotopic variations are far less than the real variations, where the maximum $\Delta^7Li_{Olivine\text{-}Cpx}$ is 17‰ (Gao et al., 2011) and ~30‰ in this study (Figure 6). Furthermore, due to the fast
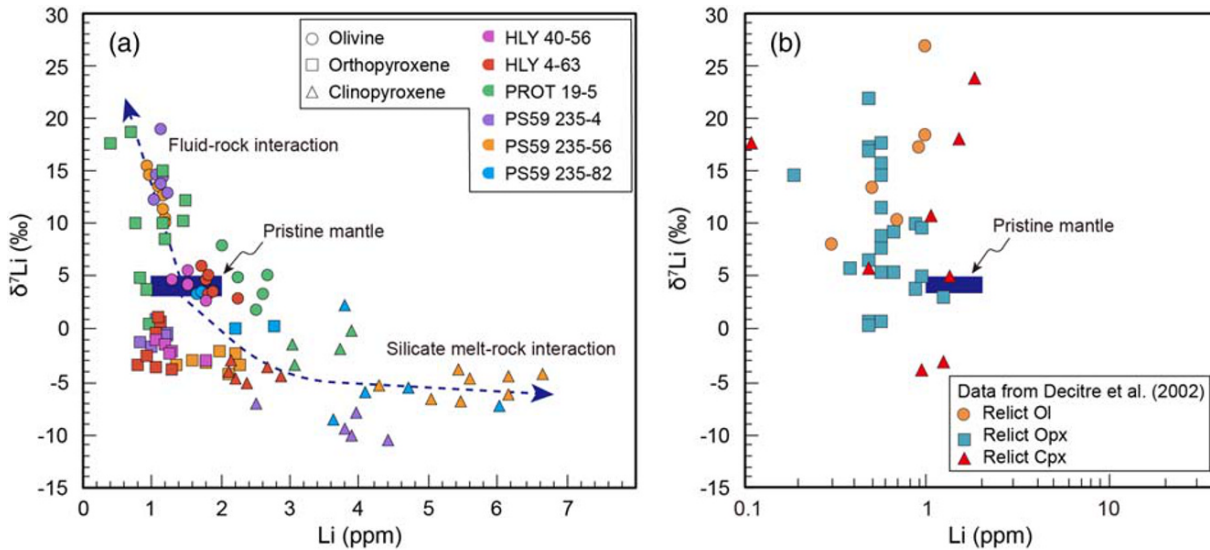
Figure 6. (a) Plot of δ^7Li versus Li content of the studied abyssal peridotites displaying two trends from the pristine mantle value. (b) In situ Li content and δ^7Li values of fresh mineral relicts in abyssal peridotite reported by Decitre et al. (2002).

diffusion of Li in Cpx, cooling-induced diffusion between olivine and Cpx at intermediate cooling rates would lead to Li zoning in olivine but nearly homogeneous Li content and δ^7Li value in Cpx (Figure 2 in Gao et al., 2011). This is inconsistent with the large variations of Li elemental and isotopic profiles of Cpx observed in this study, which indicates that Li equilibrium at millimeter scale is not reached (Figure 5).

In fact, no evidence so far shows that Li would diffuse from olivine to Cpx during cooling if they are originally in equilibrium. Although temperature-dependent Li isotopic fractionation may happen between olivine and plagioclase, such process appears to be limited between olivine and Cpx. Recent experimental studies indicate that the partition coefficient of Li between olivine and Cpx from 700°C to 1100°C varies from 1.8 to 2.2 (Yakob et al., 2012). At higher temperatures of 1300°C to 1375°C, partitioning of Li between olivine and Cpx is slightly lower at 1.2 to 1.7 (Blundy & Dalton, 2000; Ottolini et al., 2009). They together suggest no temperature dependence of KdLi olivine-cpx from 700°C to 1375°C. Field samples of mantle peridotites equilibrated at temperatures ranging from 800°C to 1400°C, likewise, have an almost invariable Li partition coefficient for olivine and Cpx at pressures of 1–4 GPa (Seitz & Woodland, 2000). Therefore, it is probable that the partition coefficient of Li between olivine and Cpx does not change much with temperature. Cooling during uplifting of the abyssal peridotites would not be able to alter Li isotopes if they are originally in equilibrium. The opposite trends of δ^7Li versus Li content of olivine and Cpx as shown in Figure 6a must be produced mainly by other processes.

5.2. Diffusion-Controlled Fractionation During Melt Impregnation

Peridotite-melt interaction is widely accepted as an ubiquitous process in mantle peridotites and could induce significant Li isotopic fractionation (Magna et al., 2008; Rudnick & Ionov, 2007; Woodland et al., 2004; Zhang et al., 2010). The alkalis, in particular, including Na and Li, in ascending melts of the mid-ocean ridges can quickly diffuse into the surrounding peridotites even at low temperatures (Lundstrom, 2000, 2003). The trend of increasing Li content coupled with decreasing δ^7Li value of Cpx and some Opx compared with that of the pristine mantle is consistent with diffusion-controlled fractionation caused by silicate-melt impregnation (e.g., Rudnick & Ionov, 2007). Because of the considerably faster diffusion rate of Li in Cpx than in olivine (Coogan et al., 2005; Parkinson et al., 2007), silicate melt impregnation in a sufficiently short period of time would induce large Li isotopic variations in Cpx and small variations in olivine.

In order to better compare the Li content and isotopic variations of Cpx and olivine at different timescales, we set up a model where Cpx or olivine (a sphere with radius a) is enclosed in a melt (another sphere with radius A). We then perform a numerical modeling using Fick's second law as the general equation for diffusion in a sphere (Crank, 1975):

$$\frac{\partial C}{\partial t} = D(T)\left(\frac{\partial^2 C}{\partial r^2} + \frac{2}{r}\frac{\partial C}{\partial r}\right)$$

where C is the Li content at position r at time t, r is the distance to the sphere center, and $D(T)$ is the temperature-dependent diffusion coefficient. The boundary conditions are set as follows:

$$\frac{\partial C}{\partial r} = 0, \ r = 0, \ r = A, \ t > 0$$

$$D_{melt}(T)\frac{\partial C}{\partial r} = D_{mineral}(T)\frac{\partial C}{\partial r}, \ r = a, \ t > 0$$

$$C_{mineral} = Kd_{mineral\text{-}melt}(T)C_{melt}, \ r = a, \ t \geq 0$$

where Kd is the partition coefficient between olivine and melt ($Kd = 0.35$; Nikogosian & Sobolev, 1997), or Cpx and melt ($Kd = 0.25$; Matsui et al., 1977). We consider the temperature of melt impregnation at 1200°C and the initial Li content and δ^7Li value of olivine (2 ppm, 4‰) and Cpx (1.1 ppm, 4‰) similar to that of the pristine mantle (Jeffcoate et al., 2007; Seitz & Woodland, 2000). The δ^7Li value of the percolating melt is 4‰ whereas the Li content of the melt varies. We modeled two cases where the initial melt has 10 ppm and 20 ppm Li, within the range of Li content in global mid-ocean ridge basalts (Tomascak et al., 2008). The diffusion coefficient of olivine is calculated according to Dohmen et al. (2010) as log $(D_{Li}) = -5.92$–$1.2847 \times 10^4/T(K)$ because the slow diffusion mechanism dominates in high-temperature magmatic systems. The diffusion coefficient of Cpx is referred to Coogan et al. (2005) that $D_{cpx} = 0.029\exp(-2.58 \times 10^5/(RT))$. The modeling details are similar to many diffusion models in previous studies (e.g., Gao et al., 2011; Parkinson et al., 2007; Richter et al., 2014). Our modeling results show that Li isotopes of Cpx can reach re-equilibrium in less than 4 days in contact with a percolating melt, whereas olivine needs tens of years to achieve re-equilibration (Figure 7). On the scale of several days, olivine Li contents and isotopic compositions remain roughly unchanged (Figures 7e and 7f). Therefore, in the cases that Li content increases a lot in Cpx but not in olivine, as the data in this study show, a short mineral-melt reaction period is required. This either indicates that melt impregnation and extraction, at least at shallow upper mantle, is a fast and efficient process, or the peridotites cool fast so that the diffusivity of Li decreases substantially with temperature. Indeed, the amount of melts generated at very-slow-spreading ridges significantly decreases with decreasing spreading rate (White et al., 2001), and melt extraction is rapid so that melts do not experience low-pressure equilibration during ascent and heterogeneity of melt compositions preserved (Kelemen et al., 1997; Langmuir et al., 1992; Niu, 1997; Stracke et al., 2006). The crystallization of olivine in the shallow upper mantle also indicates the ascent of mantle melts is accompanied by conductive cooling (Niu, 1997). Tartarotti et al. (2002) calculated that the peridotites at depths of 9–12 km in the Romanche Fracture Zone in Equatorial Atlantic have a temperature range from 750°C to 1050°C, indicative of rapid cooling after melt impregnation.

Evidence for silicate melt metasomatism in our samples includes (1) plagioclase in some peridotites, a feature of impregnation of late-stage fertile silicate melts (Figures 1i and 2d; e.g., Ciazela et al., 2015; Girardeau & Francheteau, 1993); and (2) the zoning of Y and Zr and slightly enriched REE content in Cpx (Figure 4). Calculation of Y diffusion using the diffusion coefficient of Dy at 1300°C ($D_{Dy} = 1.7 \times 10^{-19}$ m^2/s; Van Orman et al., 2001), which has a similar ionic radius with Y, shows that it generally takes ~47 ky to generate a 0.5 mm wide compositional zoning of Y in Cpx. This duration is much larger than that needed for re-equilibration of Li isotopes of Cpx at mantle temperature as discussed above and indicates that the zoning of Y and Zr was formed by multiple episodes of silicate melt metasomatism whereas the fast diffusing Li only captures the most recent event(s).

5.3. Intermineral Li Diffusion During Cooling

Because Cpx and olivine are not in Li elemental and isotopic equilibrium after melt impregnation, interdiffusion of Li would occur between them during cooling, as indicated by some concave Li isotopic profiles of Cpx (Figure 5) suggesting outward diffusion of Li (Parkinson et al., 2007). We evaluate this process using the same diffusion model as above from 1200°C to 700°C. The radius of Cpx sphere is set at 2.5 mm and that of the olivine sphere enclosing Cpx is set at 5 mm, the volume proportion of which is close to that in the abyssal peridotites. We use a maximum δ^7Li value of −25‰ and Li content of 6 ppm as the starting composition of
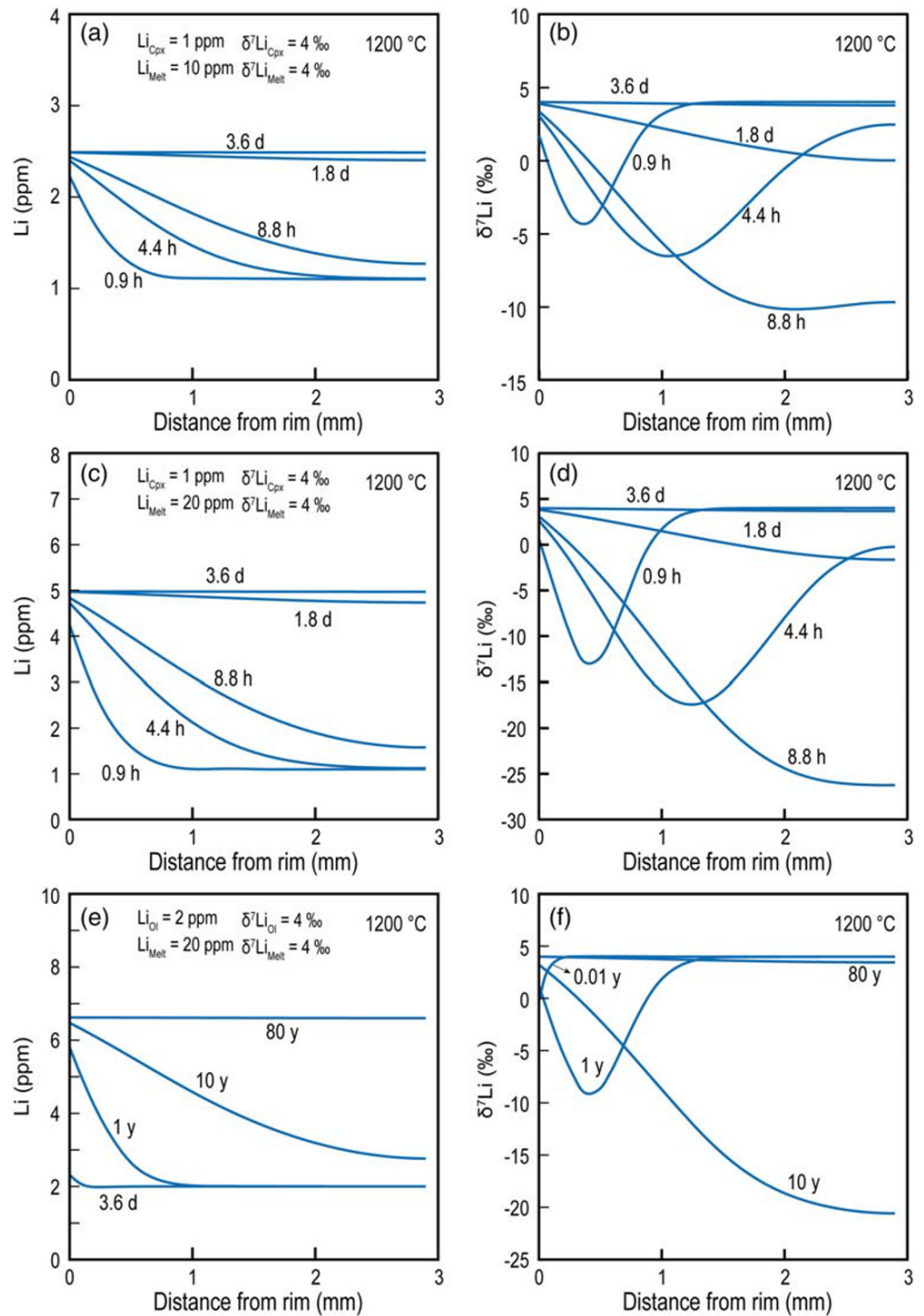
Figure 7. Numerical modeling results of Li content and δ^7Li variations during Li diffusion from the fertile silicate melt to Cpx (a–d) and olivine (e and f) at a temperature of 1200°C. Li contents of the melt were assumed to be 10 ppm (a and b) and 20 ppm (c and d), respectively. The initial Li content and δ^7Li value of olivine (2 ppm, 4‰) and Cpx (1 ppm, 4‰) were set at equilibrium mantle value (Seitz & Woodland, 2000).

Cpx, and δ^7Li value of 4‰ and Li content of 2 ppm for olivine. The modeling results show that δ^7Li values of olivine decrease for various cooling durations, whereas those of Cpx progressively increase with increasing cooling durations (Figure 8). When the cooling duration is more than ~100 years, the δ^7Li value of Cpx reaches equilibrium with that of olivine. If the cooling starts from 1000°C as some host peridotites have
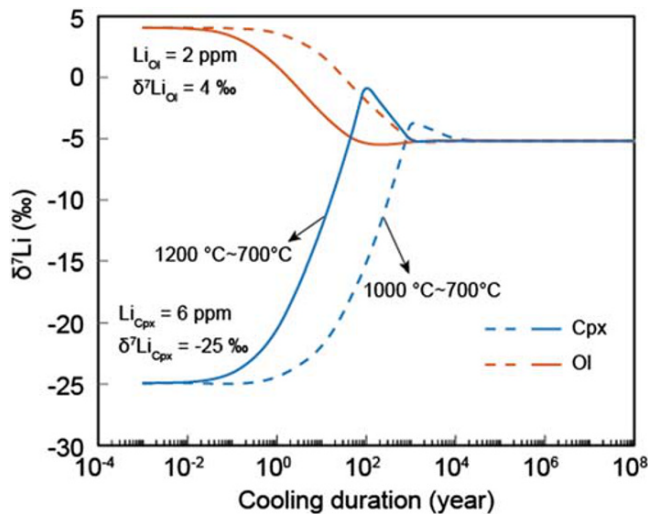
Figure 8. Predicted variations of δ^7Li values of Cpx and olivine during cooling from 1200°C to 700°C (solid line) and from 1000°C to 700°C (dashed line) through Li diffusion from Cpx to olivine. The initial Li content and δ^7Li value of Cpx were set at 6 ppm and −25‰ after peridotite-melt interaction as our data show, whereas that of olivine at 2 ppm and 4‰.

very low equilibration temperatures (Tartarotti et al., 2002), to maintain a significant change in the Cpx δ^7Li value, less than 1,000 years of cooling duration is needed (Figure 8). Therefore, the disequilibrium Li isotopic compositions of Cpx in our samples indicate a fast cooling rate of 0.3–5°C/year at the Moho boundary.

Abyssal peridotites underlying the crust can be exposed through normal faults to the seafloor where the footwalls of detachment faults are broken by land slips or cross faulting, or where the crust is sufficiently thin. Circulation of hydrothermal fluids could penetrate through these faults deep near the Moho boundary that convective cooling can result in a deeper cessation and lower degree of mantle melting (Robinson et al., 1996; VanTongeren et al., 2008). The cooling rates of abyssal peridotites at high temperatures (>1100°C) at very slow-spreading ridges are much higher than those at fast-spreading ridges and ophiolitic peridotites (Dygert et al., 2017; Dygert & Liang, 2015). The estimated cooling rate at the Moho boundary of the Samail ophiolite is ~0.3°C/year (Dygert et al., 2017) and that of the Oman ophiolite is ~0.1°C/year (VanTongeren et al., 2008). Although no data are available for the abyssal peridotites at very slow-spreading ridges at temperatures <1100°C, it is possible that the combined effects of intensified conductive cooling and deep circulation of hydrothermal fluids in the shallow upper mantle can result in fast cooling of the peridotites as it approaches close to the Moho.

5.4. Cryptic Li Diffusion in Fresh Mineral Relics During Serpentinization

As demonstrated, both melt impregnation and rapid cooling cannot be responsible for the Li isotopic characteristics of olivine. Although these abyssal peridotites are quite fresh, serpentinization can be observed along the cracks of olivine and some Opx (in sample PROT 19-5) whereas Cpx is very fresh with no alteration (Figure 2). Previous studies show that during olivine dissolution and formation of serpentine, Li can diffuse out of olivine into the fluids (Berger et al., 1988; Wimpenny et al., 2010). Because the degrees of serpentinization in our samples (Figure 2) occur in the order of olivine > Opx > Cpx (Wicks, 1969) and the ubiquitous cracks in olivine provide paths for fluid infiltration, olivine is more prone to Li exchange with fluids than Cpx. This is consistent with our Li isotopic data set that some olivine grains have very high δ^7Li values whereas most of Cpx seems not affected by this process. In some heavily serpentinized samples (e.g., PROT 19-5; Figure 1h), Opx dissolution leads to outward diffusion of Li into the hydrothermal fluids such that the Opx exhibits highly positive δ^7Li values (Figure 6a) and concave Li isotopic profile (Figure 5). For abyssal peridotites that are more heavily altered, Decitre et al. (2002) have shown that the fresh mineral relics of olivine, Cpx, and Opx have Li isotopes variably heavier and Li contents lower than the pristine mantle value (Figure 6b), the characteristics of which are consistent with diffusion of Li into the fluids during mineral dissolution and new phase precipitation. This indicates that the seemingly fresh relics of the partially serpentinized minerals start to lose Li before major elements such as Mg and Fe change significantly (Liu et al., 2017). Such cryptic Li diffusion can occur in optically fresh minerals during low-temperature fluid-rock interactions and results in increased δ^7Li values.

We carried out a diffusion modeling to investigate concentrations and isotopic changes of Li during diffusion from olivine to the fluids. The initial Li content and δ^7Li value of olivine are set similar to the mantle value ($Li_{olivine} = 2$ ppm, $\delta^7Li_{olivine} = 4$‰), whereas those of the hydrothermal fluids have variable Li contents and δ^7Li values due to interaction with the oceanic crust (Decitre et al., 2002). We therefore suppose that the Li content of the fluids is 0.5 ppm, slightly higher than that of the seawater (~0.2 ppm; Morozov, 1968), and δ^7Li value of 15‰ and 30‰, respectively, between that of the venting fluids (~8‰; Foustoukos et al., 2004) and seawater (~31‰; Rosner et al., 2007). Although the diffusion coefficient of Li in olivine at such a low temperature is unknown, it does not affect the variation trend of Li content and isotopes. The modeling results show that the fluids with δ^7Li values between 15‰ to 30‰ can produce the Li content and isotopic variations in our samples (Figure 9).

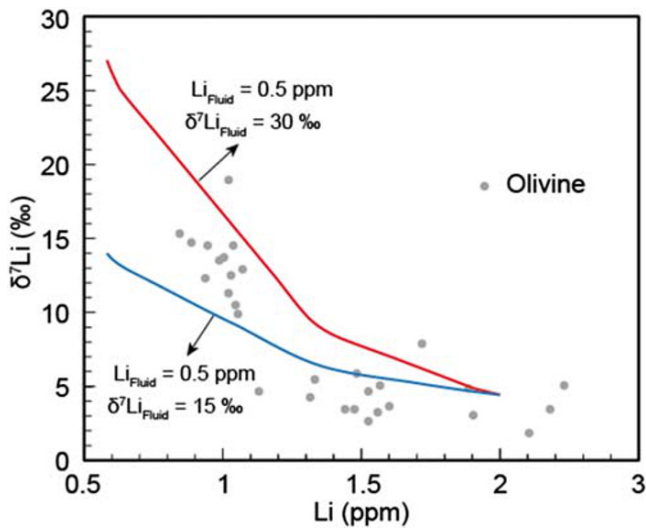**Figure 9.** Predicted variations of Li content and δ^7Li value of olivine-fluid reaction whereby Li diffuses from olivine into the hydrothermal fluids during olivine dissolution. The initial Li content and δ^7Li value of olivine were set at 2 ppm and 4‰, whereas that of the fluids at 0.5 ppm and 15‰ (blue line) and 0.5 ppm and 30‰ (red line), respectively. The Li content and δ^7Li value of olivine in this study (gray dots) fall between the two olivine-fluid interaction trends.

5.5. A Two-Stage Model for Li Variations of Abyssal Peridotites and Implications

The diverging trends in the plots of Li vs. δ^7Li of olivine, Opx, and Cpx of the abyssal peridotites compared with the pristine mantle are therefore best explained by a two-stage process (Figure 10). Before the diffusive ingress of Li, the minerals in mantle peridotites are in equilibrium with respect to concentrations and isotopes of Li, similar to those of the pristine upper mantle (Jeffcoate et al., 2007; Seitz & Woodland, 2000). Melt penetration of the variably Li-rich basaltic melt then resulted in Li diffusion from the melt to the minerals (Stage I; Figure 10a). Because the diffusion rate of Li in Cpx is significantly faster than that in olivine (Coogan et al., 2005; Dohmen et al., 2010), Li preferentially enters Cpx so that after this stage Cpx has lower δ^7Li value than olivine. Lack of Li enrichment in olivine and preservation of δ^7Li variations in Cpx indicates melt impregnation, extraction, and subsequent cooling occurred very rapidly at least at the Moho boundary of ultraslow-spreading ridges.

In the Stage II, during uplift of the peridotites on fault systems, it interacts with hydrothermal fluids (Figure 10b). Lithium isotopic fractionation between minerals and fluids is negatively correlated with temperatures (Marschall et al., 2007; Wunder et al., 2006). Since hydrothermal fluids have highly variable δ^7Li values ranging from ~0‰ to 45‰ (Decitre et al., 2002; Richard et al., 2018) and the fractionation of Δ^7Li$_{Cpx\text{-}fluid}$ varies from −1‰ to −12‰ at temperatures of 1100 to 25°C (Wunder
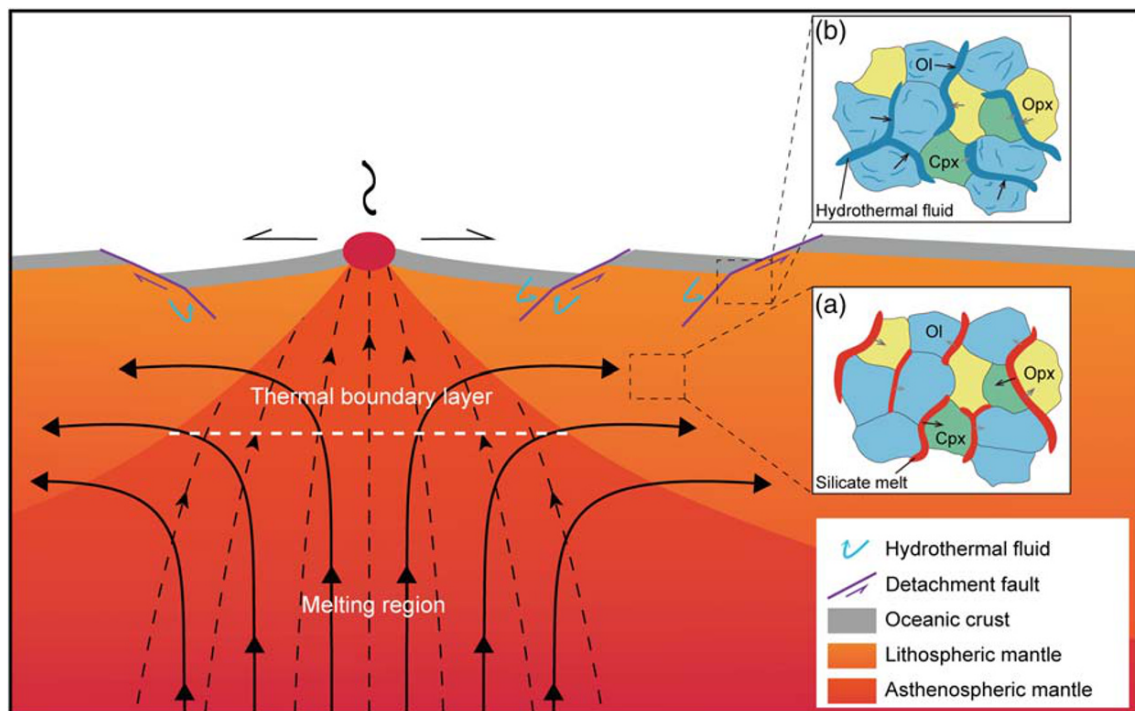

Figure 10. Schematic cartoon showing the two-stage model for Li elemental variations of abyssal peridotites (after Niu et al., 1997). Final-stage transient melt impregnation at shallow upper mantle induces Li diffusion from melt to Cpx and very little to olivine (a). The low temperature of the host peridotite and conductive cooling lead to rapid cooling that the disequilibrium Li isotopic characteristics of Cpx and olivine were preserved. Later during uplift along the detachment fault, olivine partly dissolved by the hydrothermal fluids and precipitated serpentine, during which Li diffused out of olivine into the fluids whereas the fresh and intact Cpx grains may not be affected by this process (b). The gray to black color of the arrows in a and b represent increasing extents of interaction with the melt or fluid.

et al., 2006), the Li isotopic composition of Cpx after reacting with the fluids can also be variable. Similar fractionation can be inferred for other minerals such as olivine and Opx. Because olivine is the first and foremost dissolved by the fluids (Decitre et al., 2002), cryptic Li diffusion during fluid-rock interaction frequently occurs in the order of olivine > Opx > Cpx in the optically fresh mineral relicts. The overprinting of melt-peridotite and fluid-peridotite interactions, therefore, leads to the formation of complicated Li isotopic profiles and two diverging trends of concentration of Li and δ^7Li value. The timescales of interaction largely determine the extent of variations for different minerals. It should be noted that because the Li elemental profiles on two dimensional thin sections may not necessarily transect the center of the crystals in three dimensions, the real core-to-rim variations could be even larger but in the same trend. Larger Li isotopic variations caused by melt-rock and fluid-rock interaction processes are due to higher Li contents of the melt and higher δ^7Li values of the fluid (Figures 7 and 9). Therefore, whether the Li isotopic profiles transect the real center of the minerals on three dimensions, it does not affect our interpretations.

Due to the high diffusivity and mobility, usage of Li isotopes in tracing various geological processes needs to carefully evaluate cryptic Li diffusion in visibly fresh minerals during melt-rock and high/low-temperature fluid-rock interactions, including late-stage alteration, and diffusion between disequilibrium coexisting solid phases. Marschall et al. (2007) proposed that the light δ^7Li values and high Li contents of the orogenic high-pressure metamorphic rocks were generated by diffusive influx of Li from the country rocks, instead of dehydration. The heavy δ^7Li values of the relict mineral cores in partially serpentinized mantle peridotites also indicate low-temperature serpentinization can induce Li diffusion with the fluids (Decitre et al., 2002; Jing et al., 2018). At high temperatures, Li preferentially partitions into the fluid phase relative to the solid phase (Brenan et al., 1998). Therefore, application of Li isotopes at high-temperature processes needs to consider: (1) the overprint of multi-stage melt-rock and fluid-rock interactions; and (2) the cryptic influence of high/low temperature fluids with highly variable Li isotopic compositions.

6. Conclusions

Li elemental and isotopic variations of olivine, Cpx, and Opx in abyssal peridotites of very slow-spreading ridges are due to a two-stage process that melt impregnation and fast cooling at high temperature results in an increased Li content and low δ^7Li value, whereas mineral dissolution and reprecipitation by interaction with low-temperature hydrothermal fluids lead to a decreased Li content and high δ^7Li value. The preservation of high-temperature disequilibrium Li isotopic compositions between Cpx and olivine indicates a fast cooling (0.3–5°C/year) process for the shallow upper mantle peridotites, probably caused by advective cooling of seawater and deep extension of the fault systems to the Moho boundary in ultraslow-spreading ridges where the oceanic crust is absent or very thin. Disturbance of Li isotopic systems in the visibly fresh mineral relicts requires careful consideration of the effects of high-temperature and low-temperature fluid-rock interactions.

References

Aharonov, E., Whitehead, J. A., Kelemen, P. B., & Spiegelman, M. (1995). Channeling instability of upwelling melt in the mantle. *Journal of Geophysical Research*, *100*, 20,433–20,450. https://doi.org/10.1029/95JB01307

Beck, P., Chaussidon, M., Barrat, J. A., Gillet, P., & Bohn, M. (2006). Diffusion induced Li isotopic fractionation during the cooling of magmatic rocks: The case of pyroxene phenocrysts from nakhlite meteorites. *Geochimica et Cosmochimica Acta*, *70*(18), 4813–4825. https://doi.org/10.1016/j.gca.2006.07.025

Berger, G., Schott, J., & Guy, C. (1988). Behavior of Li, Rb and Cs during basalt glass and olivine dissolution and chlorite, smectite and zeolite precipitation from seawater: Experimental investigations and modelization between 50 and 300°C. *Chemical Geology*, *71*(4), 297–312. https://doi.org/10.1016/0009-2541(88)90056-3

Blundy, J., & Dalton, J. (2000). Experimental comparison of trace element partitioning between clinopyroxene and melt in carbonate and silicate systems, and implications for mantle metasomatism. *Contributions to Mineralogy and Petrology*, *139*(3), 356–371. https://doi.org/10.1007/s004100000139

Brenan, J. M., Ryerson, F. J., & Shaw, H. F. (1998). The role of aqueous fluids in the slab-to-mantle transfer of boron, beryllium, and lithium during subduction: Experiments and models. *Geochimica et Cosmochimica Acta*, *62*(19–20), 3337–3347. https://doi.org/10.1016/S0016-7037(98)00224-5

Cannat, M., Rommevaux-Jestin, C., & Fujimoto, H. (2003). Melt supply variations to a magma-poor ultra-slow spreading ridge (Southwest Indian Ridge 61° to 69° E). *Geochemistry, Geophysics, Geosystems*, *4*(8), 9104. https://doi.org/10.1029/2002GC000480

Ciazela, J., Koepke, J., Dick, H. J., & Muszynski, A. (2015). Mantle rock exposures at oceanic core complexes along mid-ocean ridges. *Geologos*, *21*(4), 207–231. https://doi.org/10.1515/logos-2015-0017

Coogan, L. A., Kasemann, S. A., & Chakraborty, S. (2005). Rates of hydrothermal cooling of new oceanic upper crust derived from lithium-geospeedometry. *Earth and Planetary Science Letters*, *240*(2), 415–424. https://doi.org/10.1016/j.epsl.2005.09.020

Crank, J. (1975). *The Mathematics of Diffusion* (2nd ed. pp. 69–88). London: Oxford University Press.

Decitre, S., Deloule, E., Reisberg, L., James, R., Agrinier, P., & Mével, C. (2002). Behavior of Li and its isotopes during serpentinization of oceanic peridotites. *Geochemistry, Geophysics, Geosystems*, *3*(1), 1007. https://doi.org/10.1029/2001GC000178

DeMets, C., Gordon, R. G., Argus, D. F., & Stein, S. (1990). Current plate motions. *Geophysical Journal International*, *101*(2), 425–478. https://doi.org/10.1111/j.1365-246X.1990.tb06579.x

D'Errico, M. E., Warren, J. M., & Godard, M. (2016). Evidence for chemically heterogeneous Arctic mantle beneath the Gakkel Ridge. *Geochimica Et Cosmochimica Acta*, *174*, 291–312. https://doi.org/10.1016/j.gca.2015.11.017

Dick, H. J., Fisher, R. L., & Bryan, W. B. (1984). Mineralogic variability of the uppermost mantle along mid-ocean ridges. *Earth and Planetary Science Letters*, *69*(1), 88–106. https://doi.org/10.1016/0012-821X(84)90076-1

Dick, H. J., Lin, J., & Schouten, H. (2003). An ultraslow-spreading class of ocean ridge. *Nature*, *426*(6965), 405–412. https://doi.org/10.1038/nature02128

Dick, H. J. B. (1989). Abyssal peridotites, very slow spreading ridges and ocean ridge magmatism. In A. D. Saunders & M. J. Norry (Eds.), *Magmatism in the ocean basins*, *Geological Society Special Publication* (Vol. 42, pp. 71–105). London: Geological Society of London.

Dohmen, R., Kasemann, S. A., Coogan, L., & Chakraborty, S. (2010). Diffusion of Li in olivine. Part I: Experimental observations and a multi species diffusion model. *Geochimica et Cosmochimica Acta*, *74*(1), 274–292. https://doi.org/10.1016/j.gca.2009.10.016

Dygert, N., Kelemen, P. B., & Liang, Y. (2017). Spatial variations in cooling rate in the mantle section of the Samail ophiolite in Oman: Implications for formation of lithosphere at mid-ocean ridges. *Earth and Planetary Science Letters*, *465*, 134–144. https://doi.org/10.1016/j.epsl.2017.02.038

Dygert, N., & Liang, Y. (2015). Temperatures and cooling rates recorded in REE in coexisting pyroxenes in ophiolitic and abyssal peridotites. *Earth and Planetary Science Letters*, *420*, 151–161. https://doi.org/10.1016/j.epsl.2015.02.042

Foustoukos, D. I., James, R. H., Berndt, M. E., & Seyfried, W. E. (2004). Lithium isotopic systematics of hydrothermal vent fluids at the Main Endeavour Field, Northern Juan de Fuca Ridge. *Chemical Geology*, *212*(1–2), 17–26. https://doi.org/10.1016/j.chemgeo.2004.08.003

Gallagher, K., & Elliott, T. (2009). Fractionation of lithium isotopes in magmatic systems as a natural consequence of cooling. *Earth and Planetary Science Letters*, *278*(3–4), 286–296. https://doi.org/10.1016/j.epsl.2008.12.009

Gao, C., Dick, H. J. B., Liu, Y., & Zhou, H. (2016). Melt extraction and mantle source at a Southwest Indian Ridge Dragon Bone amagmatic segment on the Marion Rise. *Lithos*, *246-247*, 48–60. https://doi.org/10.1016/j.lithos.2015.12.007

Gao, Y., Snow, J. E., Casey, J. F., & Yu, J. (2011). Cooling-induced fractionation of mantle Li isotopes from the ultraslow-spreading Gakkel Ridge. *Earth and Planetary Science Letters*, *301*(1–2), 231–240. https://doi.org/10.1016/j.epsl.2010.11.003

Girardeau, J., & Francheteau, J. (1993). Plagioclase-wehrlites and peridotites on the East Pacific Rise (Hess deep) and the mid-Atlantic Ridge (Dsdp site 334)—Evidence for magma percolation in the oceanic upper mantle. *Earth and Planetary Science Letters*, *115*(1–4), 137–149. https://doi.org/10.1016/0012-821X(93)90218-X

Gu, X., Deloule, E., France, L., & Ingrin, J. (2016). Multi-stage metasomatism revealed by trace element and Li isotope distributions in minerals of peridotite xenoliths from Allègre volcano (French Massif Central). *Lithos*, *264*, 158–174. https://doi.org/10.1016/j.lithos.2016.07.019

Hellebrand, E., Snow, J. E., Dick, H. J., & Hofmann, A. W. (2001). Coupled major and trace elements as indicators of the extent of melting in mid-ocean-ridge peridotites. *Nature*, *410*(6829), 677–681. https://doi.org/10.1038/35070546

Hellebrand, E., Snow, J. E., Mostefaoui, S., & Hoppe, P. (2005). Trace element distribution between orthopyroxene and clinopyroxene in peridotites from the Gakkel Ridge: a SIMS and NanoSIMS study. *Contributions to Mineralogy and Petrology*, *150*, 486–504. https://doi.org/10.1007/s00410-005-0036-5

Ionov, D. A., & Seitz, H.-M. (2008). Lithium abundances and isotopic compositions in mantle xenoliths from subduction and intra-plate settings: Mantle sources vs. eruption histories. *Earth and Planetary Science Letters*, *266*(3), 316–331. https://doi.org/10.1016/j.epsl.2007.11.020

Jeffcoate, A. B., Elliott, T., Kasemann, S. A., Ionov, D., Cooper, K., & Brooker, R. (2007). Li isotope fractionation in peridotites and mafic melts. *Geochimica et Cosmochimica Acta*, *71*(1), 202–218. https://doi.org/10.1016/j.gca.2006.06.1611

Jing, J.-J., Su, B.-X., Xiao, Y., Martin, L., Zhang, H.-F., Uysal, İ., et al. (2018). Cryptic metasomatism revealed by Li isotopes of mantle xenoliths beneath the Thrace Basin, NW Turkey. *Journal of Asian Earth Sciences*, *166*, 270–278. https://doi.org/10.1016/j.jseaes.2018.08.025

Johnson, K. T., & Dick, H. J. (1992). Open system melting and temporal and spatial variation of peridotite and basalt at the Atlantis II fracture zone. *Journal of Geophysical Research*, *97*, 9219–9241. https://doi.org/10.1029/92JB00701

Kelemen, P., Hirth, G., Shimizu, N., Spiegelman, M., & Dick, H. (1997). A review of melt migration processes in the adiabatically upwelling mantle beneath oceanic spreading ridges. Philosophical Transactions of the Royal Society of London. Series A: Mathematical. *Physical and Engineering Sciences*, *355*(1723), 283–318. https://doi.org/10.1098/rsta.1997.0010

Langmuir, C. H., Klein, E. M., & Plank, T. (1992). Petrological systematics of mid-ocean ridge basalts: Constraints on melt generation beneath ocean ridges. In *Mantle Flow and Melt Generation at Mid-Ocean Ridges* (Vol. 71, pp. 183–280). Washington, DC: American Geophysical Union. https://doi.org/10.1029/GM071p0183

Li, X. H., Li, Q. L., Liu, Y., & Tang, G. Q. (2011). Further characterization of M257 zircon standard: A working reference for SIMS analysis of Li isotopes. *Journal of Analytical Atomic Spectrometry*, *26*(2), 352–358. https://doi.org/10.1039/C0JA00073F

Liu, C.-Z., Snow, J. E., Hellebrand, E., Brügmann, G., von der Handt, A., Büchl, A., & Hofmann, A. W. (2008). Ancient, highly heterogeneous mantle beneath Gakkel ridge, Arctic Ocean. *Nature*, *452*(7185), 311–316. https://doi.org/10.1038/nature06688

Liu, P.-P., Teng, F.-Z., Dick, H. J. B., Zhou, M.-F., & Chung, S.-L. (2017). Magnesium isotopic composition of the oceanic mantle and oceanic Mg cycling. *Geochimica et Cosmochimica Acta*, *206*, 151–165. https://doi.org/10.1016/j.gca.2017.02.016

Liu, Y., Hu, Z., Gao, S., Günther, D., Xu, J., Gao, C., & Chen, H. (2008). In situ analysis of major and trace elements of anhydrous minerals by LA-ICP-MS without applying an internal standard. *Chemical Geology*, *257*(1–2), 34–43. https://doi.org/10.1016/j.chemgeo.2008.08.004

Lundstrom, C. C. (2000). Rapid diffusive infiltration of sodium into partially molten peridotite. *Nature*, *403*(6769), 527–530. https://doi.org/10.1038/35000546

Lundstrom, C. C. (2003). An experimental investigation of the diffusive infiltration of alkalis into partially molten peridotite: Implications for mantle melting processes. *Geochemistry, Geophysics, Geosystems*, *4*(9), 8614. https://doi.org/10.1029/2001GC000224

Magna, T., Ionov, D. A., Oberli, F., & Wiechert, U. (2008). Links between mantle metasomatism and lithium isotopes: Evidence from glass-bearing and cryptically metasomatized xenoliths from Mongolia. *Earth and Planetary Science Letters*, *276*(1–2), 214–222. https://doi.org/10.1016/j.epsl.2008.09.027

Marschall, H. R., von Strandmann, P. A. P., Seitz, H.-M., Elliott, T., & Niu, Y. (2007). The lithium isotopic composition of orogenic eclogites and deep subducted slabs. *Earth and Planetary Science Letters*, *262*(3–4), 563–580. https://doi.org/10.1016/j.epsl.2007.08.005

Matsui, Y., Onuma, N., Nagasawa, H., Higuchi, H., & Banno, S. (1977). Crystal structure control in trace element partition between crystal and magma. *Bulletin de Mineralogie*, *100*, 315–324. https://doi.org/10.3406/bulmi.1977.7155

Michael, P., Langmuir, C., Dick, H., Snow, J., Goldstein, S., Graham, D., et al. (2003). Magmatic and amagmatic seafloor generation at the ultraslow-spreading Gakkel Ridge, Arctic Ocean. *Nature*, *423*(6943), 956–961. https://doi.org/10.1038/nature01704

Morozov, N. P. (1968). Geochemistry of rare alkaline elements in the oceans and seas. *Oceanology*, *8*, 169–178.

Nikogosian, I., & Sobolev, A. (1997). Ion-microprobe analysis of melt inclusions in olivine: Experience in estimating the olivine-melt partition coefficients of trace elements. *Geochemistry International*, *35*, 119–126.

Niu, Y. (1997). Mantle melting and melt extraction processes beneath ocean ridges: Evidence from abyssal peridotites. *Journal of Petrology*, *38*(8), 1047–1074. https://doi.org/10.1093/petroj/38.8.1047

Niu, Y., Langmuir, C. H., & Kinzler, R. J. (1997). The origin of abyssal peridotites: A new perspective. *Earth and Planetary Science Letters*, *152*, 251–265. https://doi.org/10.1016/s0012-821x(97)00119-2

Ottolini, L., Laporte, D., Raffone, N., Devidal, J.-L., & Le Fèvre, B. (2009). New experimental determination of Li and B partition coefficients during upper mantle partial melting. *Contributions to Mineralogy and Petrology*, *157*(3), 313–325. https://doi.org/10.1007/s00410-008-0336-7

Parkinson, I. J., Hammond, S. J., James, R. H., & Rogers, N. W. (2007). High-temperature lithium isotope fractionation: Insights from lithium isotope diffusion in magmatic systems. *Earth and Planetary Science Letters*, *257*(3–4), 609–621. https://doi.org/10.1016/j.epsl.2007.03.023

Richard, A., Banks, D. A., Hendriksson, N., & Lahaye, Y. (2018). Lithium isotopes in fluid inclusions as tracers of crustal fluids: An exploratory study. *Journal of Geochemical Exploration*, *184*, 158–166. https://doi.org/10.1016/j.gexplo.2017.10.017

Richter, F., Watson, B., Chaussidon, M., Mendybaev, R., & Ruscitto, D. (2014). Lithium isotope fractionation by diffusion in minerals. Part 1: Pyroxenes. *Geochimica et Cosmochimica Acta*, *126*, 352–370. https://doi.org/10.1016/j.gca.2013.11.008

Richter, F. M., Davis, A. M., DePaolo, D. J., & Watson, E. B. (2003). Isotope fractionation by chemical diffusion between molten basalt and rhyolite. *Geochimica et Cosmochimica Acta*, *67*(20), 3905–3923. https://doi.org/10.1016/S0016-7037(03)00174-1

Robinson, C. J., White, R. S., Bickle, M. J., & Minshull, T. A. (1996). Restricted melting under the very slow-spreading southwest Indian ridge. *Geological Society, London, Special Publications*, *118*(1), 131–141. https://doi.org/10.1144/GSL.SP.1996.118.01.07

Rosner, M., Ball, L., Peucker-Ehrenbrink, B., Blusztajn, J., Bach, W., & Erzinger, J. (2007). A simplified, accurate and fast method for lithium isotope analysis of rocks and fluids, and δ^7Li values of seawater and rock reference materials. *Geostandards and Geoanalytical Research*, *31*(2), 77–88. https://doi.org/10.1111/j.1751-908X.2007.00843.x

Rudnick, R. L., & Ionov, D. A. (2007). Lithium elemental and isotopic disequilibrium in minerals from peridotite xenoliths from far-east Russia: Product of recent melt/fluid–rock reaction. *Earth and Planetary Science Letters*, *256*(1–2), 278–293. https://doi.org/10.1016/j.epsl.2007.01.035

Seitz, H.-M., Brey, G. P., Lahaye, Y., Durali, S., & Weyer, S. (2004). Lithium isotopic signatures of peridotite xenoliths and isotopic fractionation at high temperature between olivine and pyroxenes. *Chemical Geology*, *212*(1–2), 163–177. https://doi.org/10.1016/j.chemgeo.2004.08.009

Seitz, H.-M., & Woodland, A. B. (2000). The distribution of lithium in peridotitic and pyroxenitic mantle lithologies—An indicator of magmatic and metasomatic processes. *Chemical Geology*, *166*(1–2), 47–64. https://doi.org/10.1016/S0009-2541(99)00184-9

Seyler, M., & Brunelli, D. (2018). Sodium-chromium covariation in residual clinopyroxenes from abyssal peridotites sampled in the 43°–46° E region of the Southwest Indian Ridge. *Lithos*, *302*, 142–157. https://doi.org/10.1016/j.lithos.2017.12.018

Stracke, A., Bourdon, B., & McKenzie, D. (2006). Melt extraction in the Earth's mantle: Constraints from U–Th–Pa–Ra studies in oceanic basalts. *Earth and Planetary Science Letters*, *244*(1–2), 97–112. https://doi.org/10.1016/j.epsl.2006.01.057

Su, B.-X., Gu, X.-Y., Deloule, E., Zhang, H.-F., Li, Q.-L., Li, X.-H., et al. (2015). Potential orthopyroxene, clinopyroxene and olivine reference materials for in situ lithium isotope determination. *Geostandards and Geoanalytical Research*, *39*(3), 357–369. https://doi.org/10.1111/j.1751-908X.2014.00313.x

Su, B.-X., Zhang, H.-F., Deloule, E., Vigier, N., Hu, Y., Tang, Y.-J., et al. (2014). Distinguishing silicate and carbonatite mantle metasomatism by using lithium and its isotopes. *Chemical Geology*, *381*, 67–77. https://doi.org/10.1016/j.chemgeo.2014.05.016

Sun, S. S., & McDonough, W. F. (1989). Chemical and isotopic systematics of oceanic basalts: implications for mantle composition and processes. In A. D. Saunders & M. J. Norry (Eds.), *Magmatism in the ocean basins* (Vol. 42, pp. 313–345). Geological Society, London, Special Publications. https://doi.org/10.1144/GSL.SP.1989.042.01.19

Tang, Y.-J., Zhang, H.-F., Deloule, E., Su, B.-X., Ying, J.-F., Santosh, M., & Xiao, Y. (2014). Abnormal lithium isotope composition from the ancient lithospheric mantle beneath the North China Craton. *Scientific Reports*, *4*, 4274. https://doi.org/10.1038/srep04274

Tang, Y.-J., Zhang, H.-F., Nakamura, E., Moriguti, T., Kobayashi, K., & Ying, J.-F. (2007). Lithium isotopic systematics of peridotite xenoliths from Hannuoba, North China Craton: Implications for melt–rock interaction in the considerably thinned lithospheric mantle. *Geochimica et Cosmochimica Acta*, *71*, 4327–4341. https://doi.org/10.1016/j.gca.2007.07.006

Tao, C., Seyfried, W. E., Lowell, R. P., Liu, Y., Liang, J., Guo, Z., et al. (2020). Deep high-temperature hydrothermal circulation in a detachment faulting system on the ultra-slow spreading ridge. *Nature Communications*, *11*, 1300. https://doi.org/10.1038/s41467-020-15062-w

Tartarotti, P., Susini, S., Nimis, P., & Ottolini, L. (2002). Melt migration in the upper mantle along the Romanche Fracture Zone (Equatorial Atlantic). *Lithos*, *63*(3–4), 125–149. https://doi.org/10.1016/S0024-4937(02)00116-0

Teng, F.-Z., Dauphas, N., & Watkins, J. M. (2017). Non-traditional stable isotopes: Retrospective and prospective. *Reviews in Mineralogy and Geochemistry*, *82*(1), 1–26. https://doi.org/10.2138/rmg.2017.82.1

Thiede, J. (2002). POLARSTERN ARKTIS XVII/2: Cruise report: AMORE 2001 (Arctic Mid-Ocean Ridge Expedition). In *Berichte zur Polar-und Meeresforschung, Reports on Polar and Marine Research* (Vol. 421, p. 390).

Tomascak, P. B. (2004). Developments in the understanding and application of lithium isotopes in the earth and planetary sciences. *Reviews in Mineralogy and Geochemistry*, *55*(1), 153–195. https://doi.org/10.2138/gsrmg.55.1.153

Tomascak, P. B., Langmuir, C. H., le Roux, P. J., & Shirey, S. B. (2008). Lithium isotopes in global mid-ocean ridge basalts. *Geochimica et Cosmochimica Acta*, *72*(6), 1626–1637. https://doi.org/10.1016/j.gca.2007.12.021

Tomascak, P. B., Magna, T., & Dohmen, R. (2016). *Advances in lithium isotope geochemistry* (p. 92). Berlin: Springer-Verlag. https://doi.org/10.1007/978-3-319-01430-2

Tomascak, P. B., Tera, F., Helz, R. T., & Walker, R. J. (1999). The absence of lithium isotope fractionation during basalt differentiation: New measurements by multicollector sector ICP-MS. *Geochimica et Cosmochimica Acta*, *63*(6), 907–910. https://doi.org/10.1016/S0016-7037(98)00318-4

Van Orman, J. A., Grove, T. L., & Shimizu, N. (2001). Rare earth element diffusion in diopside: Influence of temperature, pressure, and ionic radius, and an elastic model for diffusion in silicates. *Contributions to Mineralogy and Petrology*, *141*(6), 687–703. https://doi.org/10.1007/s004100100269

VanTongeren, J. A., Kelemen, P. B., & Hanghøj, K. (2008). Cooling rates in the lower crust of the Oman ophiolite: Ca in olivine, revisited. *Earth and Planetary Science Letters*, *267*(1–2), 69–82. https://doi.org/10.1016/j.epsl.2007.11.034

Warren, J., & Shimizu, N. (2010). Cryptic variations in abyssal peridotite compositions: Evidence for shallow-level melt infiltration in the oceanic lithosphere. *Journal of Petrology*, *51*(1–2), 395–423. https://doi.org/10.1093/petrology/egp096

White, R. S., Minshull, T. A., Bickle, M. J., & Robinson, C. J. (2001). Melt generation at very slow-spreading oceanic ridges: Constraints from geochemical and geophysical data. *Journal of Petrology*, *42*(6), 1171–1196. https://doi.org/10.1093/petrology/42.6.1171

Wicks, F. J. (1969). X-ray and optical studies on serpentine minerals: PhD thesis, University of Oxford, Oxford, England.

Wimpenny, J., Gíslason, S. R., James, R. H., Gannoun, A., Van Strandmann, P. A. P., & Burton, K. W. (2010). The behaviour of Li and Mg isotopes during primary phase dissolution and secondary mineral formation in basalt. *Geochimica et Cosmochimica Acta*, *74*(18), 5259–5279. https://doi.org/10.1016/j.gca.2010.06.028

Woodland, A. B., Seitz, H. M., & Yaxley, G. M. (2004). Varying behaviour of Li in metasomatised spinel peridotite xenoliths from western Victoria, Australia. *Lithos*, *75*(1–2), 55–66. https://doi.org/10.1016/j.lithos.2003.12.014

Wunder, B., Meixner, A., Romer, R. L., & Heinrich, W. (2006). Temperature-dependent isotopic fractionation of lithium between clinopyroxene and high-pressure hydrous fluids. *Contributions to Mineralogy and Petrology*, *151*(1), 112–120. https://doi.org/10.1007/s00410-005-0049-0

Yakob, J. L., Feineman, M. D., Deane, J. A., Eggler, D. H., & Penniston-Dorland, S. C. (2012). Lithium partitioning between olivine and diopside at upper mantle conditions: An experimental study. *Earth and Planetary Science Letters*, *329–330*, 11–21. https://doi.org/10.1016/j.epsl.2012.01.035

Zhang, H.-F., Deloule, E., Tang, Y.-J., & Ying, J.-F. (2010). Melt/rock interaction in remains of refertilized Archean lithospheric mantle in Jiaodong Peninsula, North China Craton: Li isotopic evidence. *Contributions to Mineralogy and Petrology*, *160*(2), 261–277. https://doi.org/10.1007/s00410-009-0476-4

Zhou, H., & Dick, H. J. B. (2013). Thin crust as evidence for depleted mantle supporting the Marion Rise. *Nature*, *494*(7436), 195–200. https://doi.org/10.1038/nature11842